

# Radio Frequency Self-Interference Cancellation in Homodyne FMCW Radar Systems

Solon J. Spiegel<sup>1</sup>, Lior Blanka<sup>2</sup>, Haim Kupershmidh<sup>2</sup>, Haim Ben Sinour<sup>2</sup>,  
Yaki Abecasis<sup>2</sup>, Adir Levi<sup>2</sup> and Moshe Haiut<sup>2</sup>

<sup>1</sup> RIO SYSTEMS, Givat Shmuel, Israel

<sup>2</sup> DSPG, Herzliya, Israel

email: solon.spiegel@rio-system.com

**Abstract**— This article presents an implementation approach for the RF self-interference cancellation in homodyne FMCW radar system. It describes the noise analysis of the transmission leakage and the benefits of self-interference cancellation. An experimental set-up was built to demonstrate the performance of the sub-system. Measurements results showed 34 dB attenuation of the CW self-interference at 1.9 GHz in the receiver channel. In practice, the multiple RF impairments in dynamic environments limit the attenuation of the transmission leakage.

**Keywords**—RF interference cancellation; FMCW; radar; self-interference cancellation; full-duplex; 5G; RF cancellers; wireless communication; transmission architecture; RF front-end; cognitive radio;

## I. INTRODUCTION

Full-duplex systems are widely employed in communication and radar applications. One of the main constraints in full-duplex systems is the transmission self-interference. Transmission leakage in the receiver band imposes limitations in the output power, frequency separation and size of the air interface. For example, communication systems demand for a wide frequency gap between the transmitter and receiver frequency bands to reduce the SNR degradation originated from cross-modulation and transmission noise leakage. The benefits and techniques for interference cancellation in radio transceivers were recently described in Refs. [1-8].

FMCW radar systems, on the other hand, suffer from noise emission and phase noise in the receiver band because of the poor isolation between the transmitter and receiver. Transmission noise leakage degrades the capability of the system to detect targets distant from the antenna. Since the echo signal is a time-delayed version of the transmitted signal with different amplitude and phase, mitigating self-interference demand for high isolation in the radio front-end.

Fig. 1 shows the simplified block diagram of a homodyne FMCW radar front-end. A single oscillator is used for coherent demodulation of the echo signal. The VCO in Fig. 1 may represent the output of a PLL synthesizer. The resultant beat frequency is proportional to the slope of the frequency ramp and the round trip distance to the target. Although not indicated in Fig. 1, an IQ demodulator might be used to convert the RF signal to the baseband. The air interface describes the topology of the antenna interface and the target.

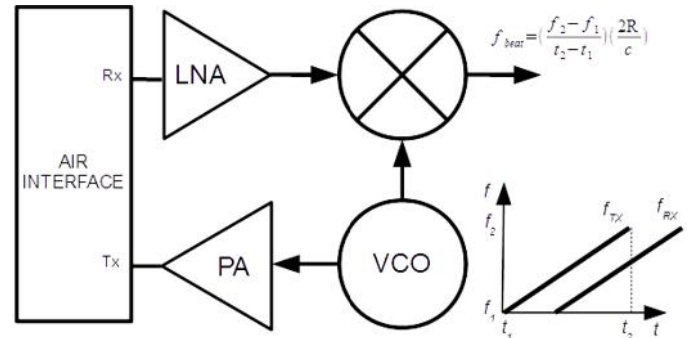


Fig. 1. Simplified block diagram of homodyne FMCW radar

Fig. 2 illustrates a conceptual block diagram of two commonly used air interface topologies for FMCW radars with single and dual antennas. The parameter  $L_1(\omega)$  represents the actual isolation in the RF front-end and  $L_2(\omega)$  the transfer function associated with the echo signal. In Fig. 2a, the  $R_X$  and  $T_X$  antennas are physically spaced from each other to guarantee sufficient isolation ( $|L_1(\omega)| \ll 0$ ). The physical separation of the antennas leads to an increase in the size of the RF front-end solution particularly at lower frequencies. A second approach consists of using a single antenna solution as shown in Fig. 2b. In this configuration, the characteristics of the circulator and the antenna matching determine the isolation between  $T_X$  and  $R_X$  terminals. In both cases, the system suffers from the limited isolation, which increase the transmission noise leakage in the receiver.

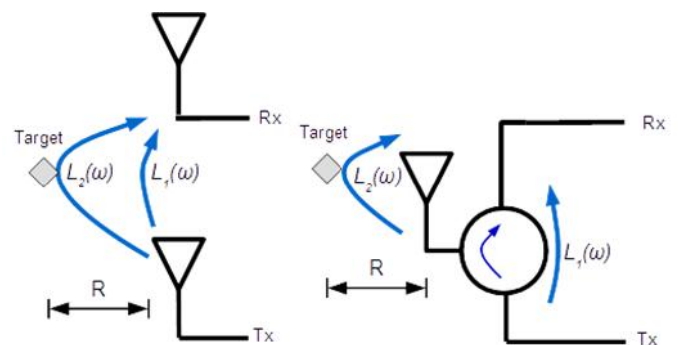


Fig. 2. Single antenna and dual antenna approaches for the air interface of FMCW radars

Self-interference cancellation technique reduces the transmission noise emission in the receiver band. When applied to FMCW radar systems, it enables the system to operate at high transmit power by reducing the phase noise and transmission leakage in the receiver band. As a result, it offer a possibility to increase in the dynamic range of FMCW radars.

The next section describes the noise analysis in homodyne FMCW receiver front-ends and the benefits of self-interference cancellation in FMCW radars. Sections III and IV describe the implementation and experimental set-up for system verification using CW waveform and, the measurement results respectively.

## II. NOISE ANALYSIS

The noise power density of the phase noise of the PLL synthesizer at the VCO output can be expressed as

$$S_{\phi_{PLL}}(\omega) = \sum_i S_{\phi_i}(\omega) |H_i(\omega)|^2 \quad (1)$$

where  $S_{\phi_i}(\omega)$  represents the noise power density of the different building blocks of the PLL synthesizer and  $H_i(\omega)$  the respective transfer function to the VCO output. The phase noise in dBc/Hz is defined as

$$L_{\phi_{PLL}}(\omega) = 10 \log(S_{\phi_{PLL}}(\omega)/P_{VCO}) \quad (2)$$

$L_{\phi_{PLL}}(\omega)$  is proportional to the output frequency due to an increase in the VCO phase noise and to the division ratio.  $P_{VCO}$  is VCO power. The phase noise is one of the main performance limiting factors in mm-wave FMCW radars.

### (a) Traditional homodyne FMCW radars

In the diagram of Fig. 1 that the conditions  $|L_{1,2}(\omega)| < 1$  and  $|L_1(\omega)| \gg |L_2(\omega)|$  are met. The noise power density at the  $R_X$  terminal of the air interface comprises of the contributions of the transmission noise power density,  $S_{TX}(\omega)$ , and the input referred thermal noise including the receiver noise figure,  $S_{RXO}(\omega)$ . The noise power density at the receiver input terminal is

$$S_{RX}(\omega) = S_{TX}(\omega) |L_1(\omega)|^2 + S_{RXO}(\omega) \quad (3)$$

The total thermal noise power density at the IF output, where  $H_{RX}(\omega)$  is the transfer function of the complete receiver chain, is defined as

$$S_{TH}(\omega) = [S_{TX}(\omega) |L_1(\omega)|^2 + S_{RXO}(\omega)] |H_{RX}(\omega)|^2 \quad (4)$$

In Eq. (4), if the noise power density is dominated by the transmission leakage,  $S_{TX}(\omega) |L_1(\omega)|^2 > S_{RXO}(\omega)$ , an increase in the transmission power level does not improve the dynamic range of the FMCW radar system as the noise floor raises with the output power, limiting the ability to detect distant targets. As a result, the isolation between the  $T_X$  and the  $R_X$  terminals, i.e.,  $L_1(\omega)$ , is a critical parameter in full duplex homodyne FMCW radar systems.

In addition to the total thermal noise in the receiver front-end, PLL synthesizer phase noise contributes significantly to the total receiver noise. From the fourrier transform of the auto-correlation between the transmitted and echo signals, the phase noise reduction in coherent FMCW radar systems at a

frequency offset ( $\Delta\omega$ ) from the carrier frequency is expressed in dBc/Hz as,

$$L_{\phi}(\Delta\omega) = 2L_{\phi_{PLL}}(\Delta\omega) \left(1 - \cos\left(\Delta\omega \frac{2R'}{c}\right)\right) \quad (5)$$

For zero length,  $R'=0$ , the phase noise is completely cancelled. The term  $2R'/c$  in (5) represents the total delay including the distance ( $R$ ) between the antenna and the target, as shown in Fig. 1, and the internal delay in the RF front-end. The phase noise power in Watt/Hz is

$$S_{\phi}(\Delta\omega) = L_{\phi}(\Delta\omega) P_{TX} |L_1(\omega)|^2 |H_{RX}(\omega)|^2 \quad (6)$$

The noise power density at the mixer output is the contributions of the thermal noise and the phase noise.

$$S_{OUT}(\omega) = S_{TH}(\omega) + S_{\phi}(\Delta\omega) \quad (7)$$

Eq. (7) shows the importance of increasing the isolation between the TX and RX terminals to reduce the contribution of the transmission noise in homodyne FMCW radars. It ultimately limits the maximum output power of the transmitter to detect targets located distant from the radar. The integration of the noise power density in (7) over the gate range defines the total noise power at the receiver.

In addition to the transmission noise leakage in the receiver, the limited isolation might cause the gain desensitization of the RF front-end. Desensitization of the gain degrades the sensitivity of the FMCW radar system.

### (b) Self-interference cancellation FMCW radars

The block diagram of the modified homodyne FMCW radar system, including self-interference cancellation is illustrated in Fig. 3. A sample of the transmission signal is applied to the receiver unit. In order to cancel the transmission noise interference, the condition (8) should be established.

$$L_1(\omega) H'_{RX}(\omega) - k(\omega) H_{SIC}(\omega) = 0 \quad (8)$$

where  $k(\omega)$  is the coupling factor,  $H_{SIC}(\omega)$  the transfer function of the cancellation sub-system and  $H'_{RX}(\omega)$  the receiver transfer function between the  $R_X$  terminal and Node A.

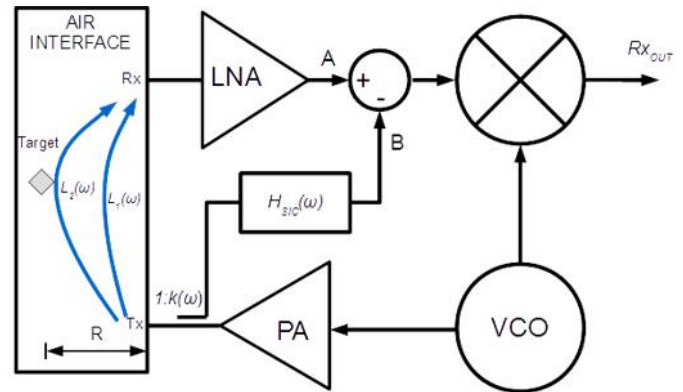


Fig. 3. Block diagram of the homodyne FMCW radar front-end with self-interference cancellation

Using the condition (8), the total thermal noise power at the IF output ( $R_{XOUT}$ ), as described in (4) can be re-written as

$$S_{TH}(\omega) = S_{RXO}(\omega)|H_{RX}(\omega)|^2 + S_{SIC}(\omega) \quad (9)$$

The new term  $S_{SIC}(\omega)$  in (9) represents the noise emission of the cancellation sub-system. Moreover, the PLL phase noise leakage defined in (6) becomes less critical in RF front-ends with high isolation between  $T_X$  and  $R_X$  terminals.

The influence of  $S_{SIC}(\omega)$  on the total noise power density is minimized with a preceding low noise amplification stage as shown in Fig. 1. One estimates that without a LNA stage, the noise power density at the output of the subtraction unit is approximately -153 dBm/Hz (condition No LNA shown in Fig. 4). This is mostly due to the noise power density at the output of the cancellation sub-system (Node B).

Consider an additional LNA with 10 dB gain, +20 dBm input 3<sup>rd</sup> order intercept point (IIP3) and 0.1 dB input IP<sub>3</sub> mismatch between the LNA and the cancellation unit. Fig. 4 shows that with interference power level below -5 dBm, the output noise at 1 MHz bandwidth is determined by the noise emission of the cancellation. For interference levels above -5 dBm, the IM<sub>3</sub> product becomes significant in comparison with the noise emission at the output of the cancellation sub-system.

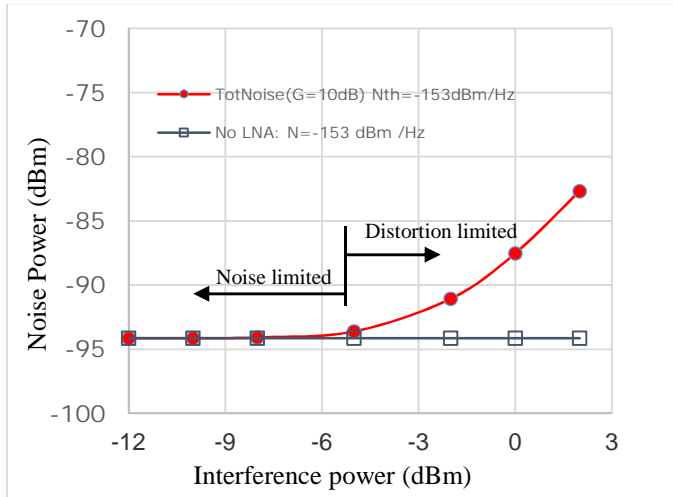


Fig. 4. Noise power at the subtraction output. At low interference power level, the total noise is dominated by the output noise of the vectro modulator.

### III. SYSTEM IMPLEMENTATION

The previous section discussed the noise analysis in homodyne FMCW radar systems and the benefits of self-interference cancellation at the receiver front-end. This section presents the implementation of RF interference cancellation sub-system. The implementation approach to estimate the transfer function  $L_1(\omega)H'_{RX}(\omega)$  for cancellation of the transmission leakage is illustrated in Fig. 5. The close loop implementation comprises of a vector modulator, amplitude and phase detectors, data converters and a programmable SoC to provide the sine and cosine functionalities in the feedback path and the connection for voltage offsets. The detailed description of the implementation was described in [1].

At the steady state, the estimates of the amplitude and phase errors,  $A_{ERR}$  and  $\theta_{ERR}$  respectively, provide the I and Q signals at the input of the vector modulator. The voltage waveform at the output of the vector modulator ( $V_B$ ) equals to

the interference waveform at the Node A ( $V_A$ ), hence, cancelling the transmission leakage term at the output of the subtraction unit. The error voltage with no impairments in the system can be expressed as

$$V_{RXOUT} = V_A - V_B \quad (10)$$

Due to multiple impairments in the system, the 35 dB attenuation of the interference is normally obtained, even though higher levels of suppression have been demonstrated in static environments. In particular, PVT variations in the amplitude and phase detectors and quantization noise in the digital to analog converter introduce impairments that degrade the amount of interference cancellation signal at RF frequencies.

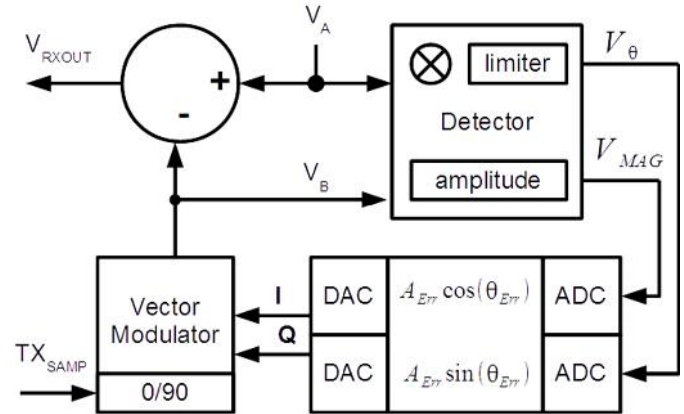


Fig. 5. Block diagram of the detailed implementation of the RF self-interference cancellation

Fig. 6 shows the experimental set-up to demonstrate the RF self-interference cancellation using a discrete implementation. The experimental set-up provides validation of the RF self-interference cancellation technique in CW systems and shed light upon the multiple RF impairments present in the realization of the RF sub-system. It also refined the values of the parameters used in the simulation model, improving its correlation with the measurement results.

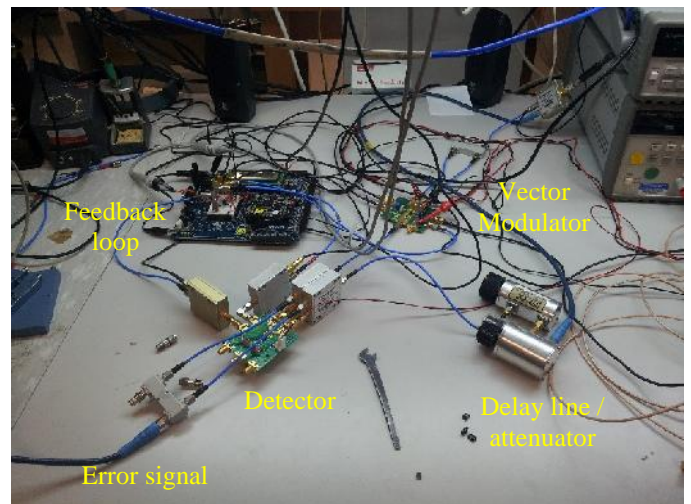


Fig. 6. Experimental set-up to demonstrate the RF self-interference cancellation

#### IV. MEASUREMENTS RESULTS

The measurement results for CW self-interference cancellation based on the experimental set-up of Fig. 6 are illustrated in Figs. 7 and 8. The interference signal consisted of a CW signal centered at 1.9 GHz. In Fig. 7, -14 dBm CW interference at 1.9 GHz was measured at the output of the subtraction unit without the interference cancellation sub-system. The measurement was taken with 50 termination at the negative port of the subtracting unit and removing the vector modulator unit.

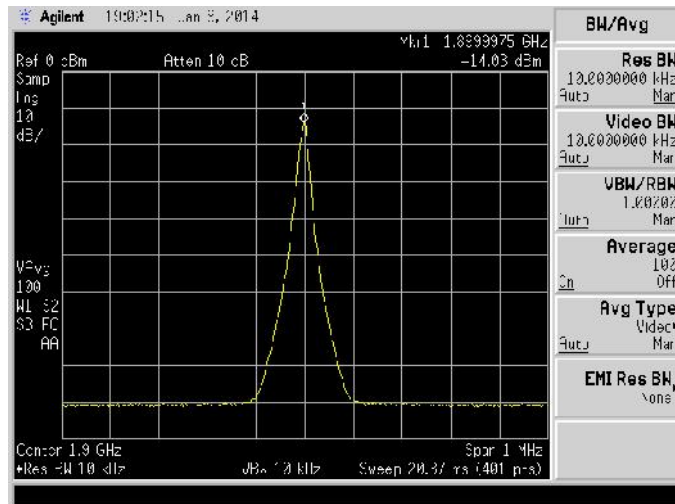
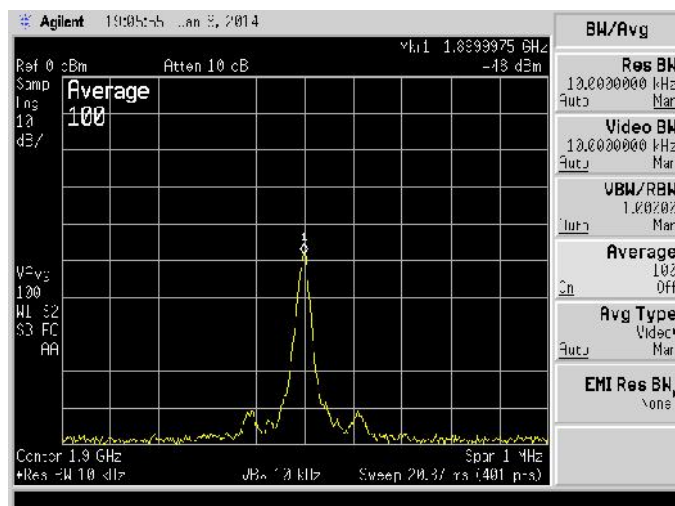


Fig. 7. Spectrum of the CW interference. The power level of -14 dBm was measured at the output of the subtraction unit without the self-interference cancellation sub-system,

The cancellation of the CW interference is shown in Fig. 8. CW interference of -48 dBm was measured at 1.9 GHz. In comparison with the -14 dBm CW power shown in Fig. 7, the power level of -48 dBm in Fig. 8 indicates 34 dB suppression of the CW interference.



Although higher attenuation has been observed under specific conditions, in practice, the multiple RF impairments Fig. 8. Output spectrum of the CW interference measured with the self-interference cancellation sub-system.

present in the implementation limits the suppression of the interference to level around 35 dB.

#### V. CONCLUSION

This paper presented a system implementation for RF interference cancellation in homodyne FMCW radar systems. Self-interference cancellation reduces the transmission leakage into the receiver enabling an increase in the dynamic range and the ability to detect targets distant from the transmission antenna.

Measurement results indicated that the self-interference cancellation technique offered 34 dB suppression of the CW transmission leakage.

#### REFERENCES

- [1] S. J. Spiegel et. Al, "Radio Frequency Interference Cancellation in Wireless Communication Systems," submitted to publication at IEEE Comcas, 2015.
- [2] S. Hong et al., "Applications of self-interference cancellation in 5G and beyond," *IEEE Communication Magazine*, pp. 114-121, February 2014.
- [3] Mikhael M. et al., "An in-band full-duplex transceiver prototype with an in-system automated tuning for RF self-interference cancellation," 1<sup>st</sup> Intl. Conf. on 5G for Ubiquitous Connectivity, pp. 110-115, Nov. 2014.
- [4] Van Liempd B et al., "RF self-interference cancellation for full-duplex," 9<sup>th</sup> Intl Conf. on Cognitive Radio Oriented Wireless Networks and Communications, pp.526-531, June 2014.
- [5] Patent US 13/625,863, "System for Allowing Co-Existence of Transceivers," Filing date 14 Sept. 2014.
- [6] Pratt, P. et al., "Digitally assisted RF filters self interference cancellation system," 44<sup>th</sup> European Microwave Conference, pp.929-932, Dec. 2014.
- [7] Wang J., Zhao H. and Tang Y., "A RF adaptive least square algorithm for self-interference cancellation in co-frequency co-time full duplex systems," IEEE Intl Conference on Communication, pp.5622-5627, June 2014.
- [8] Yang B et al., "A RF self-interference cancellation circuit for full duplex wireless communication," Proc. of Intl Symp. on Antennas & Propagation, pp.1048-1051, Oct. 2013.
- [9] He Z. et al., "Performance analysis of RF self-interference cancellation in full duplex wireless communication," *IEEE Wireless Communication Letter*, pp.405-408, Aug. 2014.



**Dr. Solon J. Spiegel** - Dr. Spiegel is currently the CTO of ISDASEMI, CEO of RIO SYSTEMS LTD and consultant for the Office of the Chief Scientist in Israel. Solon has working experience in IBM, Intel, u-blox and RAFAEL and consulting to innumerable companies in various aspects of radio technologies and integrated circuits. Dr. Spiegel holds a Ph.D. degree from the Technion and EMBA from the Swiss Federal Institute of Technology. He is senior member of IEEE and serves as chairman of IEEE-Israel solid-state society.

